Applied Physics B
Lasers and Optics

CrossMark

Flame imaging using planar laser induced fluorescence of sulfur dioxide

Rene Honza[1] · **Carl-Philipp Ding[1]** · **Andreas Dreizler[1]** · **Benjamin Böhm[1]**

Abstract Laser induced fluorescence of sulfur dioxide (SO_2-PLIF) has been demonstrated as a useful tool for flame imaging. Advantage was taken from the strong temperature dependence of the SO_2 fluorescence signal. SO_2 fluorescence intensity increases by more than one order of magnitude if the temperature changes from ambient conditions to adiabatic flame temperatures of stoichiometric methane–air flames. This results in a steep gradient of SO_2-PLIF intensities at the reaction zone and therefore can be used as a reliable flame marker. SO_2 can be excited electronically using the fourth-harmonic of an Nd:YAG laser at 266 nm. This is an attractive alternative to OH-LIF, a well-recognized flame front marker, because no frequency-doubled dye lasers are needed. This simplifies the experimental setup and is advantageous for measurements at high repetition rates where dye bleaching can become an issue. To prove the performance of this approach, SO_2-PLIF measurements were performed simultaneously with OH-PLIF on laminar premixed methane-air Bunsen flames for equivalence ratios between 0.9 and 1.25. These measurements were compared to 1D laminar flamelet simulations. The SO_2 fluorescence signal was found to follow the temperature rise of the flame and is located closer to the steep temperature gradient than OH. Finally, the combined SO_2- and OH-PLIF setup was applied to a spark ignition IC-engine to visualize the development of the early flame kernel.

1 Introduction

Flame front imaging provides important information on turbulent premixed combustion which has helped to improve our understanding of the underlying physical and chemical processes. Several approaches for flame front visualizations are available and are used on a regular base within research and the development of combustion systems [1].

The recording of flame luminosity is a simple and therefore widely used approach [2]. The spatial resolution is limited since the signal is integrated along the line-of-sight. To increase spatial resolution, planar measurement methods based on laser light sheets have been established. A simple approach is to record the Mie scattering of oil droplets that are added to the unburned flow and are consumed by the flame [3]. However, oil droplets may evaporate in front of the zone of maximum heat release and are therefore not suitable for high resolution measurements of flame structures. In terms of spatial resolution, planar laser induced fluorescence (PLIF) of radicals formed within the heat release zone, such as OH [4], HCHO [5] or CH [6] are favorable. CH is the preferable flame front marker since it is present only within the reaction zone whereas OH remains within the hot burned gases as well. Nevertheless, OH-PLIF is superior due to its high relative signal intensities and is therefore a well-established method for flame front imaging [7].

The excitation of the diatomic molecule OH requires tunable narrowband radiation in the UV spectral range. Tunable dye lasers [8] and excimer lasers [9] have been used to excite the OH molecule. These lasers were typically operated at 10 Hz providing statistically uncorrelated information. To temporally resolve transient combustion phenomena OH-PLIF has been extended into the kHz-regime [10]. The pulse energy of high speed dye lasers is still limited resulting in poor signal-to-noise ratios especially for high pressure

✉ Rene Honza
   honza@rsm.tu-darmstadt.de

1   Reactive Flows and Diagnostics (RSM), Technische
    Universität Darmstadt, Darmstadt, Germany

combustion [11]. Hence, a flame imaging method using the fourth-harmonic of an Nd:YAG laser without the need for a dye laser is advantageous for applications at high repetition rates due to significantly higher pulse energies. This reduces additionally the system's complexity.

The fluorescence of SO_2 excited at 266 nm shows a strong temperature dependency, a feature which was undesirable for exhaust gas imaging within IC-engines [12]. The presented paper exploits this temperature dependency for flame front imaging. The broadband absorbing feature of this molecule enables excitation by a fixed-frequency-quadrupled Nd:YAG laser (266 nm). SO_2 is suitable as flame front tracer since it survives flame temperatures. Within hydrocarbon flames operated with an excess of oxygen up to 20%, for example, less than 0.1% was found to react to SO_3 [13]. The red-shifted fluorescence can easily be detected and seeding levels in the order of 3000 ppm were found to provide single shot images with high signal-to-noise ratios [14].

The aim of this study is to explore the suitability of SO_2-PLIF for flame front imaging. Flame front imaging results obtained from SO_2-PLIF are benchmarked against the well-established method of OH-PLIF. Both techniques are applied simultaneously on an atmospheric, laminar jet flame. Results are compared to laminar flamelet simulations. Finally, first measurements within a spark ignition IC-engine are presented.

2 Experimental setup

2.1 SO_2 and OH-PLIF

To excite fluorescence of SO_2 one cavity of a frequency-quadrupled Nd:YAG laser (Spectra Physics, PIV400) was used providing up to 30 mJ/pulse at 266 nm. The second cavity was used to pump a dye laser (Sirah, Precision Scan, Rhodamine 6G) for OH-PLIF. The frequency-doubled output of the dye laser was tuned to 283.01 nm to excite the $Q_1(6)$ line of the A–X (1–0) transition of OH. Pulse energies were up to 20 mJ/pulse. A combination of a half-wave plate and polarizer was used to regulate the pulse energy for 266 nm, whereas angle tuning of the frequency conversion crystal (BBO) of the dye laser was used to regulate the energy of the 283 nm beam. Two separate telescopes were used to tune the divergence of each laser beam before the beams were overlapped using a polarizing beam cube. The identical laser sheet forming optics were used to form the laser-sheets for OH- and SO_2-PLIF.

The fluorescence signals were detected from opposite sides of the laser sheet perpendicularly to the laser path. For SO_2-PLIF a 16-bit ICCD camera (Princeton Instruments, PI-MAX) was used for detection, equipped with an UV lens (Halle, f = 150 mm, f/2.5) and a long pass filter (275 nm,

Asahi Spectra, ZUL0275) to block scattered laser light. The OH fluorescence emission passed through a band pass filter (Laser Components, UV-B) and was imaged by an UV lens (Nikon, UV Nikkor, f = 105 mm, f/4.5) onto an image intensifier (LaVision, IRO) that was coupled to a 12-bit CCD camera (LaVision, FlowMaster 3).

The intensifiers were gated for 300 ns bracketing the laser pulses to minimize interference from flame luminosity. The pulses were separated by 1 μs (OH followed by SO_2) to reduce cross-talk between the imaging systems. However, the broadband absorption characteristic of SO_2 leads to remaining cross-talk on the OH channel. Figure 1 shows the emission spectra for SO_2 upon excitation at 266 nm (data reproduced from [14]) and OH fluorescence following excitation at 283 nm as obtained from LIFBASE [15] simulations. The emission spectra are normalized on their maximum values. The transmission curves of the filters (measured with a Shimadzu transmission spectrometer) used in front of each detection system are overlaid. To quantify the cross-talk of SO_2 fluorescence on the OH channel, data sets were taken with and without SO_2 seeding. For both cases the dye laser was tuned to the selected excitation line of OH and to an off-resonant wavelength. The remaining signal from SO_2 was ~1% of the OH-signal for the atmospheric jet flame and around 9% within the engine.

The identical experimental setup was used for the jet flame and engine measurements. The individual settings of the laser sheet, field-of-view and pulse energies in the probe volume for these two measurements are summarized in Table 1. The optical resolution determined with a Siemens star was three pixels for both systems in both experiments and is given in physical units in Table 1.
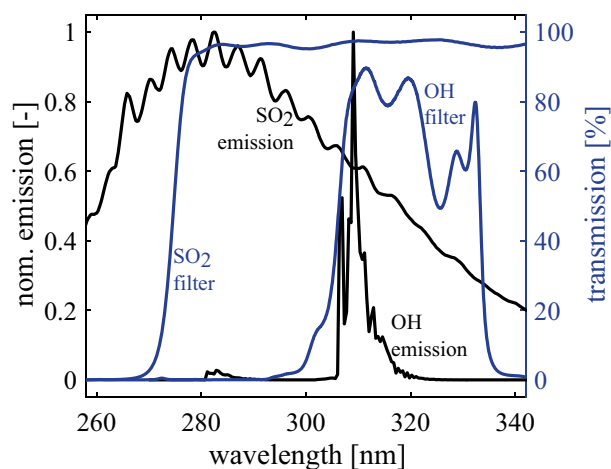

Fig. 1 LIF emission from SO_2 (data taken from [14]), OH (simulated using LIFBASE) and the transmission curves from the filters used in front of the detection systems

Table 1 Experimental parameters for both diagnostics systems in both experiments

	Jet	Engine
SO_2-PLIF		
Laser sheet thickness (mm)	0.35	0.25
Laser sheet height (mm)	2.2	15
Effective FOV (mm × mm)	24 × 2.2	15 × 16
Optical resolution (μm)	110	105
Pulse energy (mJ)	1.0	7.5
Fluence (mJ/cm^2)	129	200
SO_2 concentration (n/n%)	0.3	0.44
OH-PLIF		
Laser sheet thickness (mm)	0.45	0.35
Laser sheet height (mm)	2.2	17
Effective FOV (mm × mm)	29 × 2.2	17 × 32
Optical resolution (μm)	100	90
Pulse energy (mJ)	0.1	7.5
Fluence (mJ/cm^2)	10	126

1 UV lens 105mm f#4.5
2 UV lens 150mm f#2.5
3 BP filter 305-340nm
4 LP filter 275nm
5 correction lens
6 CCD camera
7 intensifier
8 ICCD
9 45° mirror
10 light sheet forming optics

Fig. 2 Experimental setup of the detection systems with location of the field of view (FOV). The camera orientations were perpendicular to the laser sheet
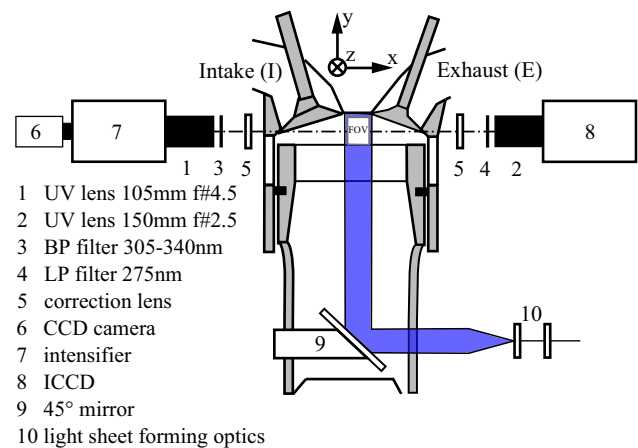
2.2 Data processing

In a first step, a 3 × 3 median filter was applied to the SO_2 and OH-PLIF raw images before correcting for background and laser beam profile. Both cameras were aligned using a self-manufactured target (backside illuminated pinhole array). Identification of corresponding pixels on both cameras was accomplished based on this target by DaVis (LaVision) providing the calibration coefficients which were used for dewarping within MATLAB (MathWorks). Finally, a 3 × 3 box filter was applied to reduce noise at the spatial scale of the resolution limit. The image mapping accuracy of both detection systems was evaluated by imaging a metal cone (similar in shape to the laminar flame) within the measurement plane with both detection systems. From 300 images, the deviation of the objects position between both systems was evaluated. The deviation was 15 μm on average with a standard deviation (STD) in the order of 30 μm, which is in the order of the pixel size.

2.3 Demonstration experiments

The capability of SO_2-PLIF for flame front imaging was evaluated by two demonstration experiments: An unconfined laminar premixed jet flame and an optically accessible spark ignition engine.

The jet burner consists of a Morel nozzle with a contraction ratio of $C_R = 4$. The ratio of the nozzle inlet diameter to the nozzle length measures $C_{LD} = 1.25$ and the exit diameter is 15 mm. The outlet velocity in the experiment was 1.2 m/s. Equivalence ratios were varied between 0.9 and 1.25. The

flow was seeded with 0.3 n/n% SO_2. Bronkhorst mass flow meters were used to control all flows individually.

The engine was an optically accessible single-cylinder spark ignition engine featuring a twin-cam, overhead-valve pent-roof cylinder head, a 55 mm high quartz-glass cylinder liner with 8 mm window extension into the pent-roof, and a Bowditch piston arrangement equipped with flat quartz-glass piston-crown window. The engine's bore and stroke are 86 mm with a displacement volume of 499.6 cm^3. The engine was operated at 800 rpm at 0.95 bar intake pressure. A homogenous stoichiometric methane/air mixture was provided by port-fuel injection of methane ~1.1 m upstream the intake valves. SO_2 was seeded into the flow ~1.6 m upstream the intake valves and was set to 0.44 n/n%. Spark timing was set to 19° crank angle before top dead center. The engine operated in skip-fire mode (60 s fired, followed by 60 s motored). Data acquisition started after 10 s of fired engine operation. Images were taken at 10° crank angle before top dead center where the in-cylinder pressure was 12 bar and the polytropic temperature was estimated to be 590 K. Figure 2 shows more details on the experimental setup. A comprehensive description of the test bench is given in [16].

2.4 Influence of tracer concentration and laser fluence

The dependence of SO_2 fluorescence intensity on seeding concentration and laser fluence was investigated in the burned gas region of the stoichiometric, laminar flame. No changes within the OH-gradient shape as well as the OH intensities were observed for the variation of SO_2 concentrations between 0 and 0.3 n/n%. Figure 3a shows the fluorescence intensity for an SO_2 concentration variation. The laser fluence was set to 400 mJ/cm^2 and the equivalence ratio was 1.0. The intensity scales perfectly linear with concentration.
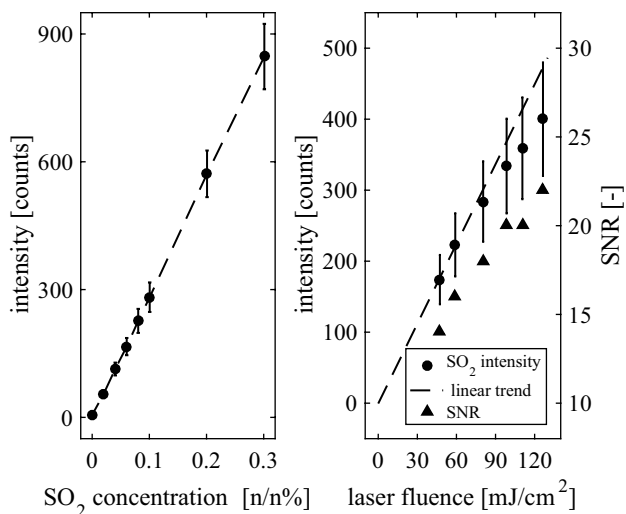
Fig. 3 Fluorescence intensities depending on tracer concentration (**a**) and laser fluence (**b**) within a stoichiometric methane air flame
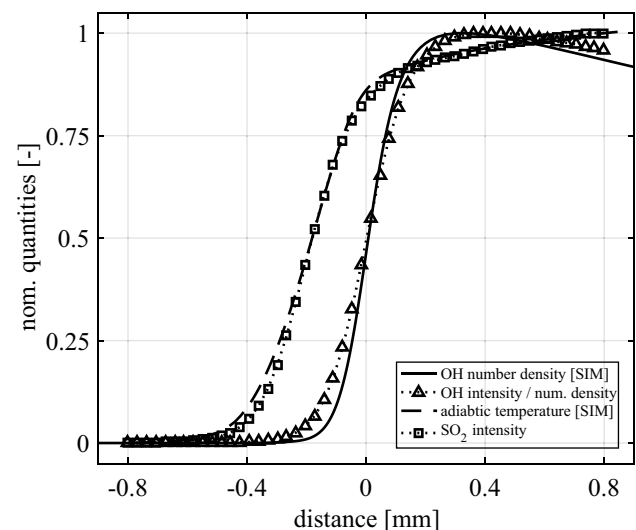

Fig. 4 Simulated OH- and temperature profiles of the laminar jet flame together with measured OH- and SO_2 intensities. All profiles are normalized using the respective minimum and maximum value

Figure 3b shows a power scan for a fixed SO_2 concentration of 0.3 n/n%. The pulse energies were varied with the half-wave plate and recorded by an energy meter during the measurements (Coherent). The fluorescence signal scales linearly with laser fluence up to ~60 mJ/cm^2 before saturation starts. Within this work the laser fluence was set to 129 mJ/cm^2 for high signal-to-noise ratio while keeping the deviation from linearity within 20%. In favor of high SNR the same approach was chosen for the OH measurements. The intensity scaled linearly with laser fluence up to 6.5 mJ/cm^2. Final measurements were conducted with 10 mJ/cm^2 (10% deviation from linearity).

3 Results

3.1 Laminar premixed jet flame

To evaluate the performance of SO_2-LIF for flame front imaging, results of the simultaneous SO_2 and OH-LIF measurements from the laminar premixed jet are compared to 1D laminar flamelet simulations (Chem 1D, [17]). For an equivalence ratio of 1 Fig. 4 shows normalized OH and SO_2 profiles perpendicular to the flame front that are determined from 300 individual snapshots. Since the laminar flame was not absolutely stationary, the steepest gradient of the extracted OH-profiles was set to $x = 0$ mm (horizontal coordinate) before averaging. The steepest OH-gradient was also used to overlay the simulation and experimental results. The slope of the measured OH-profile is not as steep as for the simulations due to the limited spatial resolution of the detection system (~100 μm). All profiles are scaled between the lowest (unburned gas) and the highest value (burned gas)

within the range plotted (−0.8 mm to 0.8 mm). Whereas OH concentrations are zero in the unburned gas, SO_2 signals were in the order of 15 counts and 270 counts in the burned gas region, respectively. The temperature range was within 300–2020 K. The SO_2 fluorescence signal follows the (adiabatic) temperature rise of the flame within ~40 μm which is below the resolution limit of the measurements. The distance between the steepest OH and SO_2 gradient was computed for all individual 300 images. The average distance was 193 μm on the left hand side (LHS) of the flame and 208 μm on the right hand side (RHS) with a standard deviation of 60 μm. This gives confidence in the alignment of the optical setup and the overlap of the laser-sheets. For the present conditions the OH-profiles, which are commonly used as flame marker, show a larger distance to the maximum temperature gradient than the SO_2 profiles.

For equivalence ratios between 0.9 and 1.25, Fig. 5 shows the distance between the steepest OH and temperature gradient as obtained from the 1D-simulations (Chem1D) together with the experimentally determined distance between the OH and SO_2 profiles (100 individual snapshots). These results clearly show how the distance between OH and temperature increases for increasing equivalence ratios. The distance increases by ~30% when changing the equivalence ratio from 1 to 1.25. However, SO_2 follows the temperature gradient regardless of equivalence ratio variations with the distance remaining below 100 μm.

The signal-to-noise ratio (SNR) was determined from a 50×50 pixel region within the burned gas and was 22 for SO_2 and 18 for OH.
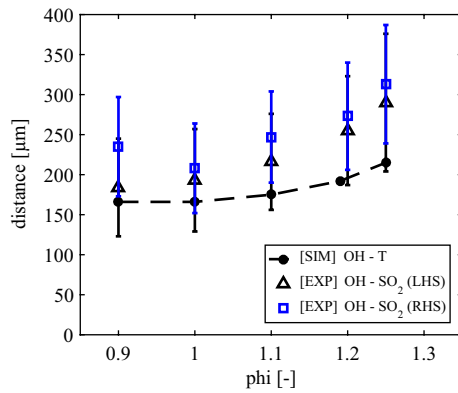
Fig. 5 Distances depending on equivalence ratio

3.2 Optically accessible engine

For the investigated engine operational condition the flame thickness is expected to decrease compared to the investigated atmospheric laminar jet flame due to the higher pressure [18]. Figure 6 shows individual snapshots of SO_2 and OH of the early flame kernel as recorded with
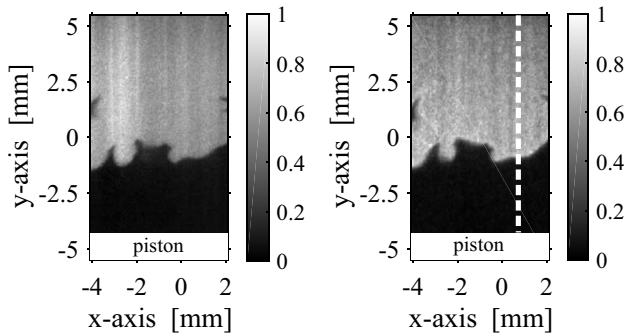

Fig. 6 Flame visualization within the SI engine using simultaneous SO_2 LIF (*left*) and OH-LIF (*right*)
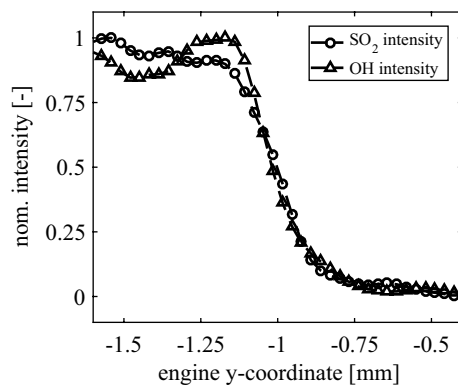

Fig. 7 SO_2- and OH-LIF profiles from the engine measurements taken along the dashed line shown in Fig. 6

the simultaneous SO_2- and OH-PLIF setup. The distance between OH and SO_2 was evaluated along profiles perpendicular to the flame front. Figure 7 shows the OH and SO_2 profiles along the dashed line highlighted in Fig. 6. A statistical analysis using 80 samples revealed an average distance of 12 μm with a standard deviation of 29 μm which is below the spatial resolution limit. The SNR was calculated from a 50×50 pixel area within the burned gas region and was 15 for SO_2 and 13 for OH, respectively.

4 Conclusions

In this work the suitability of SO_2 as a flame front marker was investigated. SO_2 profiles across laminar flames stabilized at a jet burner were compared to simultaneous OH-LIF measurements and laminar flamelet calculations. The SO_2 LIF signal was observed to follow the temperature rise within the heat release zone much closer than the OH-LIF signal. For a stoichiometric flame, the distance between the OH-LIF signal and temperature was ~160 μm whereas the distance between SO_2 and temperature profiles was offset by ~40 μm and hence small in comparison to the optical resolution of ~100 μm. The addition of SO_2 did not change the flame in respect of its shape and size. Finally, the feasibility of SO_2-LIF for flame front detection was demonstrated within an optically accessible IC-engine. The SO_2 and OH-LIF signals moved closer towards each other due to the elevated in-cylinder pressure. The average distance between both signals was observed to be 12 μm which was below the resolution limit of the detection systems. The pulse energy for SO_2 LIF within the engine was 7.5 mJ and resulted in a signal-to-noise ratio of ~15. Thus, SO_2-LIF is a promising tool for flame front imaging in IC-engines at high repetition rates where pulse energies of 1–2 mJ are readily available with state-of-the-art laser systems at 266 nm without the complexity of an additional dye laser.

References

1. J. Wolfrum, Lasers in combustion. Symp. (Int.) Combust. **27**(1), 1–41 (1998)
2. P.G. Aleiferis, A.M.K.P. Taylor, J.H. Whitelaw, K. Ishii, Y. Urata, Cyclic Variations of Initial Flame Kernel Growth in a Honda VTEC-E Lean-Burn Spark-Ignition Engine, SAE Paper 2000-01-1207, 2000
3. C. Heeger, B. Böhm, S.F. Ahmed, R. Gordon, I. Boxx, W. Meier, A. Dreizler, E. Mastorakos, Statistics of relative and absolute

velocities of turbulent non-premixed edge flames following spark ignition. Proc. Combust. Inst. **32**(2), 2957–2964 (2009)

4. B. Peterson, E. Baum, B. Böhm, A. Dreizler, Early flame propagation in a spark-ignition engine measured with quasi 4D-diagnostics. Proc. Combust. Inst. **35**(3), 3829–3837 (2015)

5. S. Boeckle, J. Kazenwadel, T. Kunzelmann, D.-I. Shin, C. Schulz, Single-shot laser-induced fluorescence imaging of formaldehyde with XeF excimer excitation. Appl. Phys. B **70**(5), 733–735 (2000)

6. V. Bergmann, W. Meier, D. Wolff, W. Stricker, Application of spontaneous Raman and Rayleigh scattering and 2D LIF for the characterization of a turbulent CH 4/H 2/N 2 jet diffusion flame. Appl. Phys. B Lasers Opt. **66**(4), 489–502 (1998)

7. E.P. Hassel, S. Linow, Laser diagnostics for studies of turbulent combustion. Meas. Sci. Technol. **11**(2), R37 (2000)

8. M.J. Dyer, D.R. Crosley, Two-dimensional imaging of OH laser-induced fluorescence in a flame. Opt. Lett. **7**(8), 382 (1982)

9. W. Ketterle, M. Schaefer, A. Arnold, J. Wolfrum, 2D single-shot imaging of OH radicals using tunable excimer lasers. Appl. Phys. B Photophys. Laser Chem. **54**(2), 109–112 (1992)

10. C. Kittler, A. Dreizler, Cinematographic imaging of hydroxyl radicals in turbulent flames by planar laser-induced fluorescence up to 5 kHz repetition rate. Appl. Phys. B **89**(2–3), 163–166 (2007)

11. S.H.R. Müller, B. Böhm, M. Gleißner, S. Arndt, A. Dreizler, Analysis of the temporal flame kernel development in an optically accessible IC engine using high-speed OH-PLIF. Appl. Phys. B **100**(3), 447–452 (2010)

12. K. Fukui, T. Fujikawa, M. Tohyama, Y. Hattori, K. Akihama, 2-D Internal EGR Distribution Measurements in an Engine by Laser-Induced Fluorescence. SAE Int. J. Engines **6**(1), 289–299 (2013)

13. G.M. Johnson, C.J. Matthews, M.Y. Smith, D.J. Williams, Distribution of sulfur species in the burnt gas of fuel-rich propane-air flames. Combust. Flame **15**(2), 211–214 (1970)

14. V. Sick, Exhaust-gas imaging via planar laser- induced fluorescence of sulfur dioxide. Appl. Phys. B Lasers Opt. **74**(4–5), 461–463 (2002)

15. J. Luque, & D.R. Crosley, *LIFBASE: Database and spectral simulation program*. Version 1.5, SRI International report MP 99-009 (SRI International, Menlo Park, CA, 1999)

16. E. Baum, B. Peterson, B. Böhm, A. Dreizler, On the validation of LES applied to internal combustion engine flows. Flow, Turbul Combust **92**(1–2), 269–297 (2014)

17. CHEMID, *A one-dimensional laminar frame code*. (Eindhoven University of Technology, 2002)

18. J. Göttgens, F. Mauss, N. Peters, Analytic approximations of burning velocities and flame thicknesses of lean hydrogen, methane, ethylene, ethane, acetylene, and propane flames. Symp. (Int.) Combust. **24**(1), 129–135 (1992)